Bulletin of Engineering Geology and the Environment (2022) 81: 331
https://doi.org/10.1007/s10064-022-02832-7

ORIGINAL PAPER

Evaluation of geological model uncertainty caused by data sufficiency using groundwater flow and land subsidence modeling as example

Shih-Jung Wang[1] · Quoc Cuong Nguyen[1,2] · Yu-Chen Lu[3] · Yonatan Garkebo Doyoro[4,5,6] · Duc-Huy Tran[1]

Received: 4 January 2022 / Accepted: 16 July 2022 / Published online: 26 July 2022

Abstract

Uncertainty in hydrogeological modeling has recently received attention. It has been reported that the geological model is one of the primary sources of uncertainty. The present study developed a synthetic geological model (SGM) based on the geological characteristics in Taiwan as the baseline. Simulated geological models with various levels of data sufficiency were assessed based on multiple borehole numbers, with and without the incorporation of geological knowledge, and a combination of geophysical data with borehole data. The models were used in groundwater flow and land subsidence simulations. The results from the models were assessed and compared by calculating the root-mean-square error and coefficient of determination (R^2) corresponding to SGM to evaluate the geological model uncertainty. The results show that a model based on data from 17 boreholes that incorporates geological knowledge for a 300 m × 300 m site provides an acceptable assessment of land subsidence. The geological model that incorporates geological knowledge extensively improves the numerical models, demonstrating that geological knowledge is necessary for deriving geological models. The model using geophysical data with correction based on data from at least 13 boreholes provided better results compared with those obtained using data from various numbers of boreholes or only geophysical data. This study demonstrates that additional data can significantly decrease the uncertainty in geological and numerical models. The results can be used by engineers and researchers to decide on a suitable strategy for engineering geology projects based on the precision requirements and budget. They can also help minimize risk when modelers and stakeholders make decisions.

Keywords Geological model uncertainty · Data sufficiency · Geological knowledge · Borehole number · Geophysical data assimilation · Land subsidence

Introduction

Uncertainty in hydrogeological modeling has recently received attention (Lelliott et al. 2009; Benedek and Molnár 2013; Li et al. 2016; Mahmoudpour et al. 2016; Juang et al. 2019; Tran et al. 2022). Its analysis has become an integral part of hydrogeological simulations (Marinoni 2003; Shi et al. 2008; Guillaume et al. 2012). Many studies have shown that the primary sources of uncertainty in groundwater hydrogeological simulations are (1) numerical model settings, (2) data input, and (3) the geological model (Refsgaard et al. 2006; Hassan et al. 2008). Several techniques have been developed for estimating the uncertainties in model results, such as the quantification of the uncertainty in boundary and initial conditions using data assimilation techniques (Fan et al. 2016; Liu et al. 2019; Qi and Liu 2019) and simultaneous data assimilation and parameter estimation (Moradkhani et al. 2005; Vrugt et al. 2005; Tao et al. 2020). However, because these studies used a single model (changes in model structure were not

✉ Shih-Jung Wang
sjwang@ncu.edu.tw

1 Graduate Institute of Applied Geology, National Central University, Taoyuan, Taiwan

2 DRAGON - Mekong Institute, Can Tho University, Can Tho, Vietnam

3 Institute of Materials Science & Engineering, National Central University, Taoyuan, Taiwan

4 Earth System Science, Taiwan International Graduate Program (TIGP), Academia Sinica, Taipei, Taiwan

5 Department of Earth Science, National Central University, Taoyuan, Taiwan

6 Department of Applied Geology, School of Natural Sciences, Adama Science and Technology University, Adama, Ethiopia

considered), the effects of structural deficiencies on model results were unaccounted for. Additional data may reduce some types of uncertainty, such as parametric and boundary uncertainty (Gallagher and Doherty 2007; Shi et al. 2008; Guillaume et al. 2012). Other types of uncertainty, such as geological uncertainty, have not been fully evaluated. Most studies on uncertainty analysis have focused on data input and model settings (Refsgaard et al. 2006). However, studies have found that geological models are a leading source of uncertainty (Neuman 2003; Bredehoeft 2005; Refsgaard et al. 2012; Yeh et al. 2021; Tran et al. 2022). Significant effort has been devoted to developing methods for determining hydrogeological conceptual models, which can be used to estimate model uncertainty (Rojas et al. 2008; Boyd et al. 2019). However, there is no simple method for evaluating the effects of geological model uncertainty, which is often ignored in groundwater applications (Bredehoeft 2003, 2005; Neuman 2003; Carrera et al. 2005; Refsgaard et al. 2006; Shi et al. 2012; Yao et al. 2021).

Several methods are available for simulating geological models, each with its own benefits and drawbacks. For example, data from many boreholes are required to achieve high accuracy in simulations of geological models using a stochastic Markov random field (Li et al. 2016; Qi et al. 2016; Wang et al. 2017a; Zhao et al. 2020). The transition probability matrix indicates the correlation between the spatial distributions of materials in boreholes with the horizontal and vertical directions. Thus, the boundaries of the strata generated with this approach tend to be linear, which degrades the simulation results in complex geological settings (Wang et al. 2018). In most cases, geological data are sparse and geological profiles are complex due to long-term structural deformation. Subsurface profiles are commonly simulated based on the spatial interpolation of geological information from borehole data (Chiles et al. 2004; Mahmoudpour et al. 2016; Wang et al. 2017b). However, these methods generally neglect the geological uncertainty in the model and do not consider geological knowledge. Højberg and Refsgaard (2005) reported that geological uncertainty is extremely important in simulations of groundwater flow. Gong et al. (2020) found that the geological model can significantly influence the numerical results for a groundwater flow system if an insufficient number of boreholes are used to construct the geological model. In practice, the geological settings are often invisible, and the interpretation derived from the models developed based on limited information represents only part of the complete picture. Therefore, the model results are significantly influenced by the quality of the input data (Lelliott et al. 2009).

Numerous studies have analyzed uncertainty in land subsidence and groundwater flow modeling (e.g., Wang et al. 2015). However, relatively few have considered the uncertainty in geological models. The present study thus focuses on evaluating geological model uncertainty based on the sufficiency of input data during the construction of a geological model for groundwater flow and land subsidence modeling. Geological models with (1) various numbers of boreholes (to evaluate the influence of borehole density on the simulated geological model), (2) with and without the incorporation of geological knowledge (to evaluate the suitability of incorporating geological knowledge into a geological model), and (3) with and without geophysical data assimilation (to evaluate the effectiveness of combining different and complementary data types to minimize geological model uncertainty) were assessed. The results of this study can be used to reduce the uncertainty of geological models with various levels of data sufficiency. They can also minimize risk when modelers and stakeholders make decisions.

Methodology

This study investigates the effect of the uncertainty in geological models with various levels of data sufficiency on groundwater flow and land subsidence (Table 1). The baseline is a synthetic geological model (SGM) developed in this study. The numerical results from each geological model were compared with those of SGM. To evaluate the effect of the number

Table 1 List of simulated geological models

Parameter	Simulated cases
Borehole number	1 borehole with incorporation of geological knowledge
	5 boreholes with incorporation of geological knowledge
	9 boreholes with incorporation of geological knowledge
	13 boreholes with incorporation of geological knowledge
	17 boreholes with incorporation of geological knowledge
Geological knowledge	17 boreholes without incorporation of geological knowledge
Geophysical data	Only ERT data
	ERT data with correction based on data from 9 boreholes
	ERT data with correction based on data from 13 boreholes
	ERT data with correction based on data from 17 boreholes

of boreholes, data from 1 to 17 boreholes were taken from SGM to reconstruct a geological model (i.e., simulated geological model). The horizon ID method was used in the geological model simulation with correction based on geological knowledge. To evaluate the effect of geological knowledge, the horizon ID method was used in the geological model simulation without correction based on geological knowledge for the case with 17 boreholes. To evaluate the effect of geophysical data assimilation, electrical resistivity tomography (ERT) was used in SGM to assess the clay thickness. The original estimated clay thickness and that corrected based on data from 17 boreholes with the cokriging method were input into the Subsidence and Aquifer-System Compaction (SUB) package in MODFLOW, respectively, to estimate the influence on land subsidence simulations. The adopted methods and related concepts are described below.

Synthetic geological model construction

The diamond-square algorithm (DSA) (Fournier et al. 1982) was used to generate the random terrain height in SGM. This algorithm, also called the random midpoint displacement fractal, cloud fractal, or plasma fractal, is used for generating realistic-looking terrain and procedural textures. The DSA process can be divided into two main steps: the diamond step and the square step. The calculation procedure of DSA is as follows.

1. Create a $(2^n+1)\times(2^n+1)$ matrix, where n is the number of DSA iterations, with the given initial values (heights) for the four corners.
2. (Diamond step) Calculate the midpoint of the square array in the matrix with the average value from the four corners plus a random value.
3. (Square step) Calculate the midpoint of the diamond array in the matrix with the average value from the four corners plus a random value.
4. Repeat the diamond and square steps n times.

Although a random geological surface can be obtained with this algorithm, many geological structures (e.g., synclines, anticlines, discrete patterns, faults) cannot always be successfully generated by DSA. The trend of the target geological structure should be considered. Therefore, we developed a numerical code to generate a realistic-looking SGM that considers the trend of the geological structure and the DSA results. The formulation of a random terrain can be expressed by:

$$H(x,y) = T(x,y) + d(x,y) \quad (1)$$

where H is a random elevation of a geological surface, T is the trend function of the geological surface, and d is the elevation calculated from DSA with the random value in steps 2 and 3 having zero mean and standard deviation. The trend of each geological surface can be determined based on the assumed geological scenario. A realistic-looking geological model can then be easily generated by Eq. (1).

Methods for simulating geological models

Horizon ID method

The horizon ID method in the groundwater modeling system (GMS) assigns an ID for each material in a borehole. This method can help construct a geological model with the layer system from borehole data. Horizon numbering may have gaps. A primary triangulated irregular network (TIN) must be created or imported into the GMS for the horizon ID method. The primary TIN defines the boundaries of formed solids. The density of the triangles in solids is controlled by the mass of the triangles in the primary TIN.

First, the user or system assigns horizon IDs to each segment of a borehole. The horizon IDs represent the aquifer or aquitard to which the materials belong in the depositional sequence (from bottom to top) in a borehole. Second, the primary TIN is defined based on a standard triangulation algorithm (Tsai 1993; De Loera et al. 2010). The boundaries of solids are based on the TIN's boundaries. Third, the horizon surface is created by interpolating the horizon elevations. Fourth, the surfaces of the horizons are intersected. Each TIN is intersected with all other TINs. Fifth, the elevation of each horizon in the primary TIN is adjusted. Finally, one solid is built for each horizon based on the TIN elevations from the above steps (Lemon and Jones 2003).

This study developed simulated geological models with and without the incorporation of geological knowledge. Without geological knowledge, the horizon ID method automatically connects and extends the formation based on the assigned IDs of the strata. However, auto-connection is not able to recognize the order of the formation and may connect a given material to different layers, and auto-extension does not consider the continuity of the formation, extending the strata to a default length. Interpolation and extrapolation methods can also strongly affect the simulated geological model. Therefore, geological knowledge has been used to correct the connection and extension of the strata based on the order of the formations and the continuity concept of a geological material, respectively. A suitable interpolation or extrapolation method was also selected based on the simulated results obtained with geological knowledge. Some areas around the boundary need model extrapolation due to a lack of borehole data, which leads to high uncertainty in groundwater flow and land subsidence modeling results. Increasing the number of boreholes or combining some boreholes outside the region of interest can decrease the

extrapolation error and uncertainty in the model. Geological knowledge was also used to correct the non-horizontal formations around the boundary.

Electrical resistivity tomography method

ERT is a non-invasive geophysical technique for imaging subsurface structures based on electrical resistivity measurements. The electrical resistivity method injects an electric current into the ground. The current flows through different subsurface media results in a variation in electrical resistivity values, which can be used to determine the type of material. The variation in measured electrical resistivity is related to lithology, mineral composition, water content, porosity, permeability, and pore water composition (Archie 1942). The recovery ability of electrical resistivity imaging methods (electrode configurations) varies with subsurface material variation (Doyoro et al. 2021; Nyári and Kanlı 2007). Water content can considerably vary the electrical properties of clay material (Nyári et al. 2010). In addition, electrical resistivity is sensitive to electrolyte and soil-fluid interface chemistry, and the grain surface conduction becomes significant when clay minerals are present (Kanli and Neducz 2015; Tildy et al. 2017). Because ERT is highly sensitive to the presence of clay content, clay layer/zone information can be obtained from electrical resistivity data.

A forward simulation is a good approach for outlining the linkage between geological models and geophysical methods. Eleven two-dimensional geological cross sections were extracted at 30-m intervals from the three-dimensional (3D) SGM (Fig. 1). Then, two-dimensional electrical resistivity synthetic models were constructed using the electrical resistivity values of lithologic units. This study applied the Wenner–Schlumberger configuration because it is moderately sensitive to lateral and vertical variations and has a high signal-to-noise ratio. This study applied 76 electrodes with a 4-m spacing for surface electrical resistivity probing. The apparent electrical resistivity was calculated by solving partial differential equations (Rubin and Hubbard 2006) using finite element modeling with 1 m × 1 m structured meshes. The inverted model was recovered using smoothness-constrained least-squared inversion, which attempts to minimize the squares of the spatial changes of the model resistivity and is adequate for gradually varying resistivity environments (Loke et al. 2003).

Governing equations

Governing equation of groundwater flow

MODFLOW, a finite-difference groundwater flow code developed by the United States Geological Survey, can be used in the GMS 3D Grid module to create a groundwater

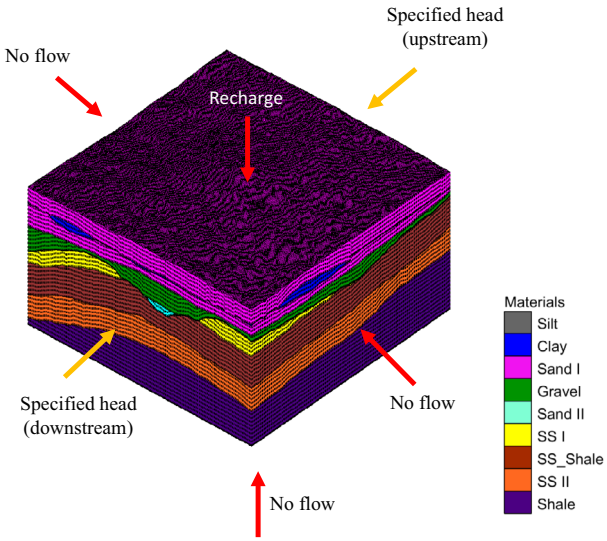

Fig. 1 Synthetic geological model in GMS and boundary conditions. The two specified heads represent the upstream (north) and downstream (south), respectively. To control the groundwater flow from the upstream to the downstream, the east and west boundaries of the model were set as no-flow boundaries. Because of the low permeability bedrock, the bottom boundary of the model was set as a no-flow boundary. The top boundary was set to a constant recharge. *SS* sand stone

flow model (McDonald and Harbaugh 1988). The core mathematical model of MODFLOW is the following partial differential equation (Rushton and Redshaw 1979), which describes the 3D movement of groundwater flow through porous media:

$$\frac{\partial}{\partial x}\left(k_x\frac{\partial h}{\partial x}\right)+\frac{\partial}{\partial y}\left(k_y\frac{\partial h}{\partial y}\right)+\frac{\partial}{\partial z}\left(k_z\frac{\partial h}{\partial z}\right)-W=S_s\frac{\partial h}{\partial t} \quad (2)$$

where h is the hydraulic head [L], W is the volumetric source per unit volume that represents sources and sinks of water [T^{-1}], t is time [T], S_s is the specific storage of the porous material [L^{-1}], and k_x, k_y, and k_z are the hydraulic conductivity values along the x, y, and z directions, respectively [L/T].

Governing equation of land subsidence

Land subsidence was simulated using the SUB package based on MODFLOW-2000 (Harbaugh et al. 2000). SUB is based on the Interbed Storage Package, version 2 (IBS2) (Leake 1990). It considers the delay in the release of groundwater from a compressible interbed. Both elastic and inelastic sediment compaction is computed. Only vertical displacement is considered in the simulation. Horizontal displacement occurs near pumping wells or local heterogeneities in aquifer systems in response to pumping. Seasonal recharge/discharge tends to be highly limited

Table 2 Material properties in SGM

Condition	Layer number	Lithology	Electrical resistance (Ω·m)	Horizontal hydraulic conductivity (m/d)	Specific yield*
Unconsolidated layers	1	Silt	300	0.05	0.08
	2	Clay	20	0.0001	0.03
	3	Sand I	150	35	0.21
	4	Gravel	500	100	0.35
	5	Sand II	150	10	0.21
Consolidated layers	6	Sandstone I	2000	0.1	0.27
	7	Sandstone/shale	1500	0.001	0.25
	8	Sandstone II	3000	0.01	0.27
	9	Shale	300	0.0001	0.26

* Modified from Johnson (1967)

(Hoffmann et al. 2003). The local horizontal displacement slightly contributes to the overall change in groundwater storage for regional groundwater flow and land subsidence models. SUB estimates both the expansion and compaction of the interbed and aquifers in each model layer and sums the vertical displacement values at the ground surface. The compaction in response to the hydraulic head decrease in unconsolidated aquifer systems, as reported in several studies (Terzaghi 1925; Meinzer 1928; Jacob 1940). The effective stress is related to pore water pressure and the total stresses caused by overburden as follows:

$$\sigma^{'} = \sigma - u \tag{3}$$

where $\sigma^{'}$ is the effective or intergranular stress [$ML^{-1}\ T^{-2}$], σ is the geostatic stress (a load caused by overlying saturated and unsaturated sediments and water) [$ML^{-1}\ T^{-2}$], and u is the pore water pressure in the sedimentary matrix [$ML^{-1}\ T^{-2}$].

The theory assumes that deformation is vertical and the total stress is constant. In SUB, the vertical subsidence is based on the change in effective stress, which is assumed to change with the hydraulic head. Land subsidence is calculated as:

$$\Delta b = S_{sk} b \Delta h \tag{4}$$

where Δb is the layer compaction [L], S_{sk} is the skeletal specific storage [L^{-1}], b is the original thickness of the layer [L], and Δh is the change in the hydraulic head [L]. Two separate values are used to account for the marked change of the skeletal specific storage when the effective stress changes:

$$\begin{cases} S_{ske} & \sigma'_{zz} < \sigma'_{zz(max)} \\ S_{skv} & \sigma'_{zz} \geq \sigma'_{zz(max)} \end{cases} \tag{5}$$

where S_{ske} is the elastic skeletal specific storage [L^{-1}], S_{skv} is the inelastic skeletal specific storage [L^{-1}], and $\sigma'_{zz(max)}$ is the preconsolidation stress [$ML^{-1}\ T^{-2}$].

Numerical model settings

Initial and boundary conditions and stress period settings

The domain of the constructed SGM is 300 m × 300 m (Fig. 1). The specified head boundary condition (Dirichlet boundary condition) was set at the upstream (north) and downstream (south). To control the groundwater flow from the upstream to the downstream in the aquifer, the east and west boundaries of the model were set as no-flow boundaries (Neumann boundary condition). Because of the low permeability of the bedrock, the bottom boundary of the model was also set as a no-flow boundary. The top boundary was set according to the recharge condition.

The transient state condition was considered in the groundwater flow model. Fifty stress periods, each with a duration of 90 days (total of 4500 days), were used. The

Table 3 Parameters of clay interbed

Parameter	Vertical hydraulic conductivity (K_v)	Elastic specific storage (S_{ske})	Inelastic specific storage (S_{skv})	Elastic skeletal storage coefficient (S_{ke})	Inelastic skeletal storage coefficient (S_{kv})
Unit	m/d	1/m	1/m	–	–
Value	1×10^{-4}	1×10^{-3}	1×10^{-2}	3.38×10^{-5}	9.79×10^{-3}

Modified from Hong (2011)

stress periods of the land subsidence model were the same as those for the groundwater flow model. Pumping began after 90 days. The initial groundwater level for each grid was equal to the top layer elevation. The initial land subsidence of all grids was set to zero in the land subsidence model.

Sources and sinks

The sources and sinks in this study include groundwater extraction and recharge. A well in MODLFOW can be a source or sink. Wells are defined by assigning a pumping rate to a selected cell. Wells can be injection wells (positive flow rate) or extraction wells (negative flow rate). The WEL package was used to set up pumping wells in the model. To avoid bias in pumping and focus on discussing the effect of the geological model on the estimation of land subsidence, the pumping wells were set up in each cell of the sand I layer in the model with a total extraction quantity of 4500 m^3/day, which represents uniform pumping for the whole area. This pumping quantity was set to obtain a maximum land subsidence of around 5 cm.

The recharge (RCH) package was used to simulate recharge to an aquifer due to rainfall and infiltration. Recharge is typically defined for each stress period for each vertical column in the grid by specifying a recharge value. The recharge value represents the quantity of water from the surface that goes into the groundwater system. The recharge in this study was set up at all of the highest active cells in the model with a recharge rate of 0.0009 m/day for all stress periods (Wang et al. 2021).

Parameter settings

Because this study focuses on assessing the uncertainties in the geological model, the parameters for each material adopted in this study were assumed to be constants (see Table 2). The vertical hydraulic conductivity (VK) was assumed to equal 1/10 the horizontal hydraulic conductivity (HK) (i.e., HK/VK = 10). In this study, clay was assumed to be the only compressible material. The parameters of the clay interbed are listed in Table 3.

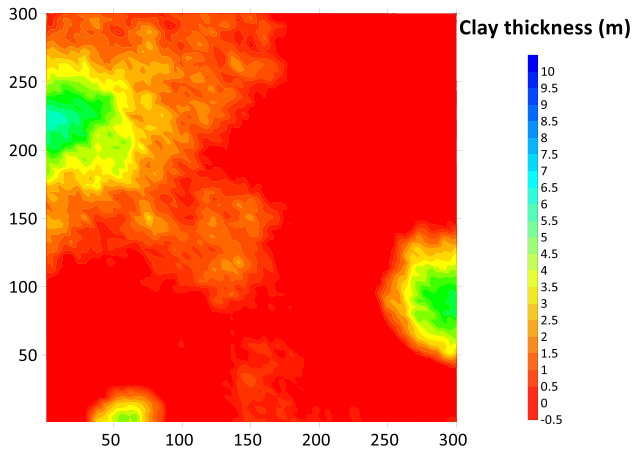

Fig. 2 Distribution of clay thickness in SGM model

Results and discussion

Synthetic geological model

The developed SGM is shown in Fig. 1 and its information is listed in Table 2. It consists of various topographies, e.g., anticline strata (layer nos. 8 and 9), an anticline stratum with erosion (layer no. 7), an anticline stratum with a discrete phase (layer no. 6), a horizontal stratum (layer no. 3), and horizontal strata with a discrete phase (layer nos. 1, 2, 4, and 5). The lithologies of the strata are listed as unconsolidated formations, namely silt (no. 1), clay (no. 2), sand I (no. 3), gravel (no. 4), and sand II (no. 5), and consolidated rock formations, namely sandstone I (no. 6), sandstone and shale interbedded (no. 7), sandstone II (no. 8), and shale (no. 9). The geological structure of SGM was set to be a moderately complex configuration with the mesoscale condition, which is similar to the foothills or hilly areas in western Taiwan. The elevation of SGM was assumed to decrease from north (upstream) to south (downstream). The geological structure of this model includes:

1. Strata that contain unconsolidated formations and consolidated rock formations
2. Strata that contain various significant permeabilities
3. A rock bed inclination that is dominated by a geological structure that is assumed to be an anticline

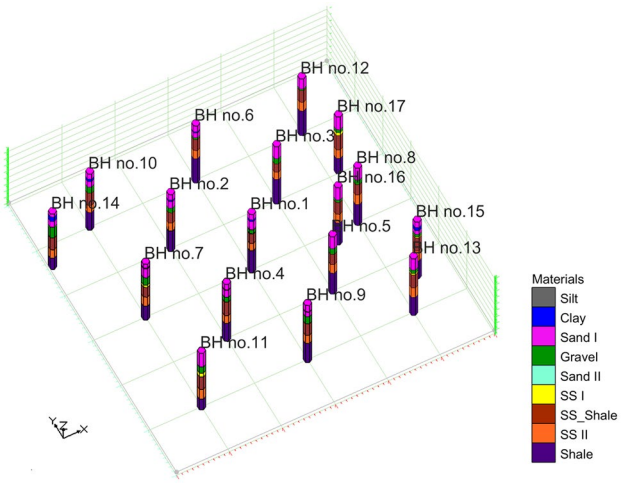

Fig. 3 Boreholes extracted from SGM to construct simulated geological models. Simulated geological models that adopted data from 1, 5, 9, 13, and 17 boreholes used boreholes no. 1, nos. 1–5, nos. 1–9, nos. 1–13, and nos. 1–17, respectively

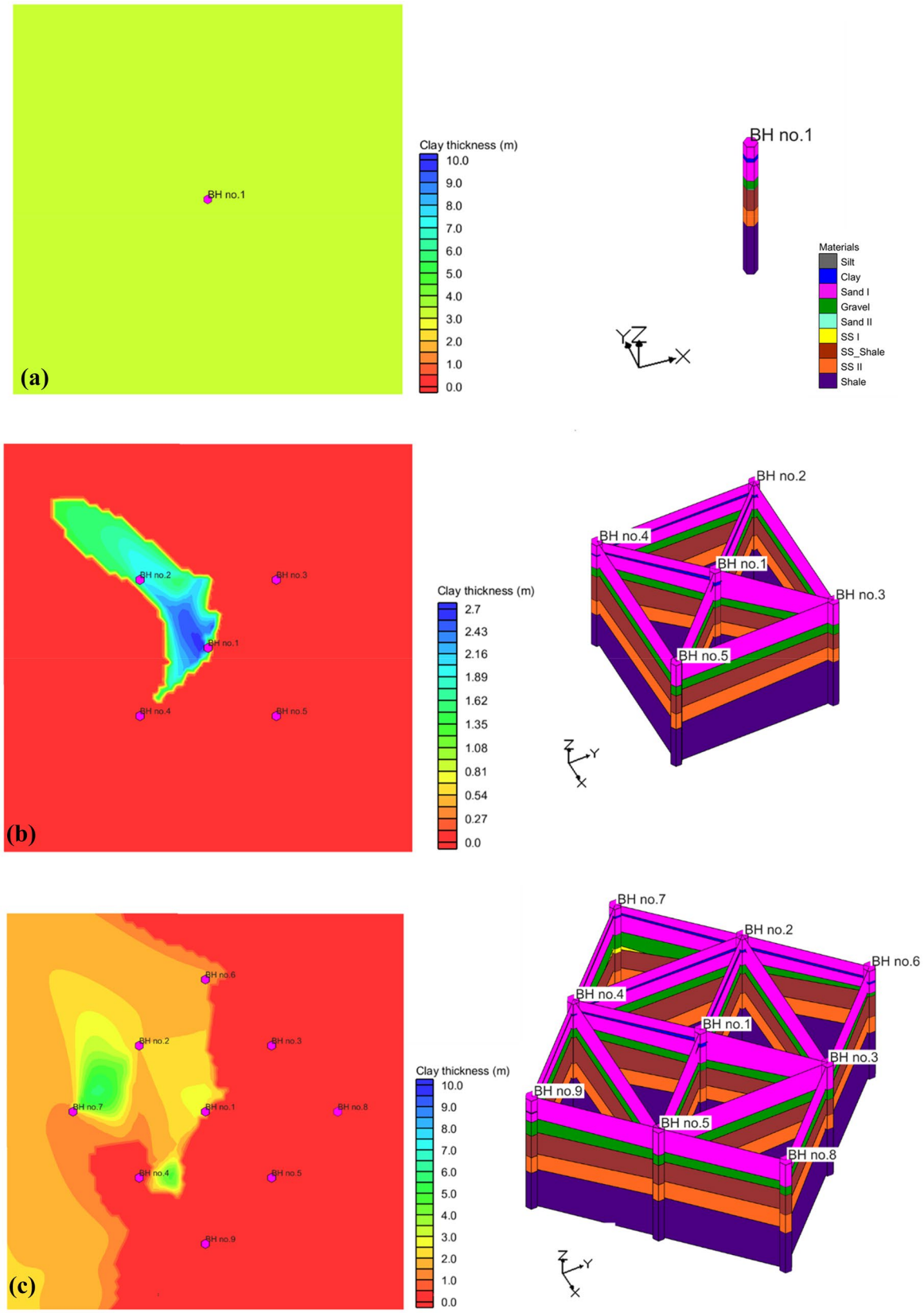

Fig. 4 Distribution of clay thickness in simulated geological models (left) and geological cross sections (right) obtained using horizon ID method with data from various numbers of boreholes with incorporation of geological knowledge. Results for **a** 1, **b** 5, **c** 9, **d** 13, and **e** 17 boreholes

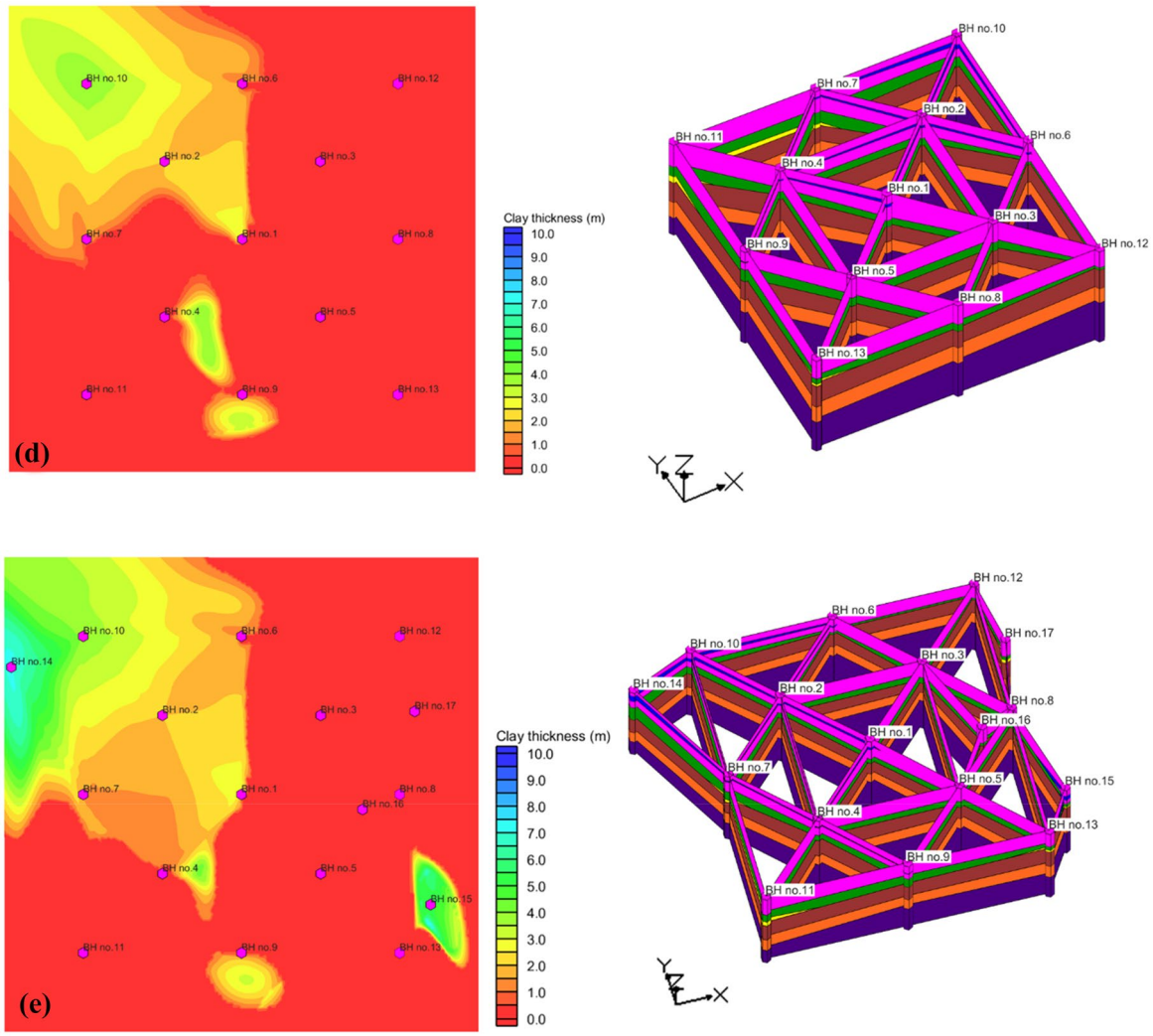

Fig. 4 (continued)

4. A realistic-looking elevation of the ground surface

A 3D geological model with a multilayer system was built by extracting the elevation data from the SGM subsurface and inputting them into the GMS (Fig. 1). The model consisted of all layers except the silt layer at the top layer of the model in the numerical simulation. The silt layer was taken out of the model because it was too thin and discontinuous, making the boundary condition setting difficult. Clay material in the model was considered an inelastic medium, which typically results in high land subsidence. Clay thickness in SGM is shown in Fig. 2.

Simulated geological models

Simulated geological models were constructed based on various levels of data sufficiency. The results of groundwater flow and land subsidence obtained with these models are compared to those of SGM using an error assessment.

Effect of number of boreholes

Data from 1, 5, 9, 13, and 17 boreholes were extracted from SGM, respectively (Fig. 3). The borehole placement rule adopted in this study was based on the concept used in an

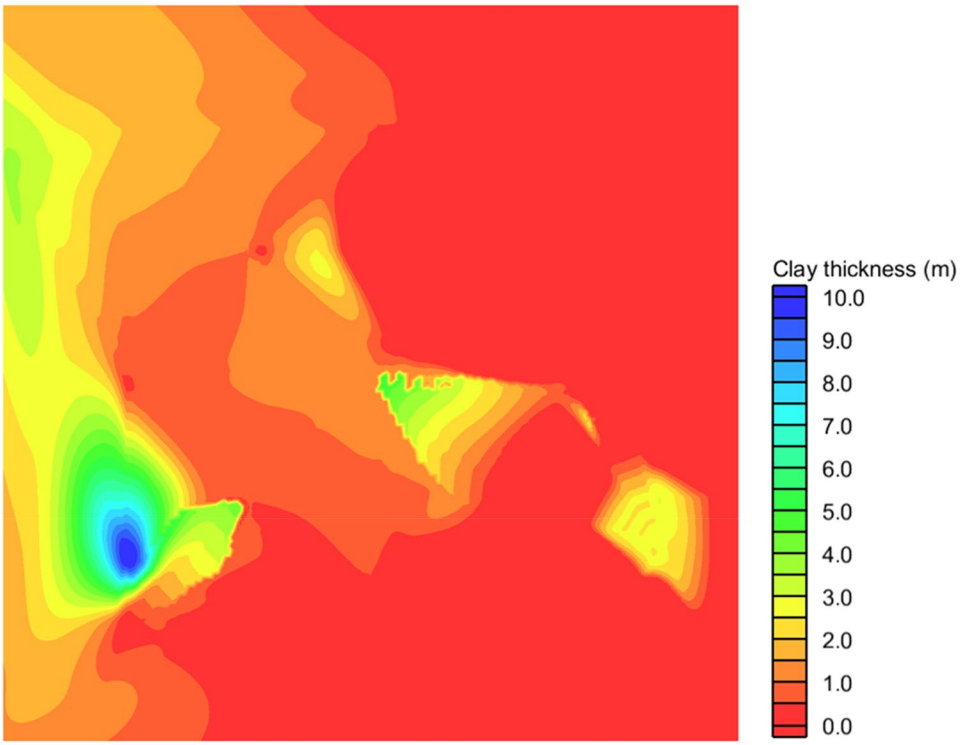

Fig. 5 Distribution of clay thickness in simulated geological model based on data from 17 boreholes without incorporation of geological knowledge

engineering site, with the assumption that the main target was at the center. For a study site, if only one borehole is required, it is commonly set at the center (no. 1). If the main target is at the center, additional boreholes (nos. 2 to 5) are placed around the target, i.e., near borehole no. 1. If more boreholes can be used, two sets of boreholes (nos. 6 to 9 and nos. 10 to 13, respectively) are placed from the center to an adjacent area. Then, because the boreholes uniformly occupy the study area (except at the boundary), boreholes nos. 14 to 17 are placed randomly.

The horizon ID method was used to simulate geological models based on data from various numbers of boreholes. The cross sections, minimum thickness of each layer (materials), strata around the boundary, and spatial distribution of the materials were assessed and calibrated based on geological knowledge to reflect a realistic situation. Some of the cross sections were modified based on geological concepts in SGM, such as anticline strata (layer nos. 8 and 9), an anticline stratum with erosion (layer no. 7), an anticline stratum with a discrete phase (layer no. 6), a horizontal stratum (layer no. 3), and horizontal strata with a discrete phase (layer no. 1).

Five simulated geological models were constructed, as shown in Fig. 4. Data from 1 or 5 boreholes were insufficient for capturing the distribution of clay (compared with Fig. 2). Data from 9 to 17 boreholes were sufficient for constructing an approximate clay distribution. The distribution of clay thickness became closer to that of SGM with increasing

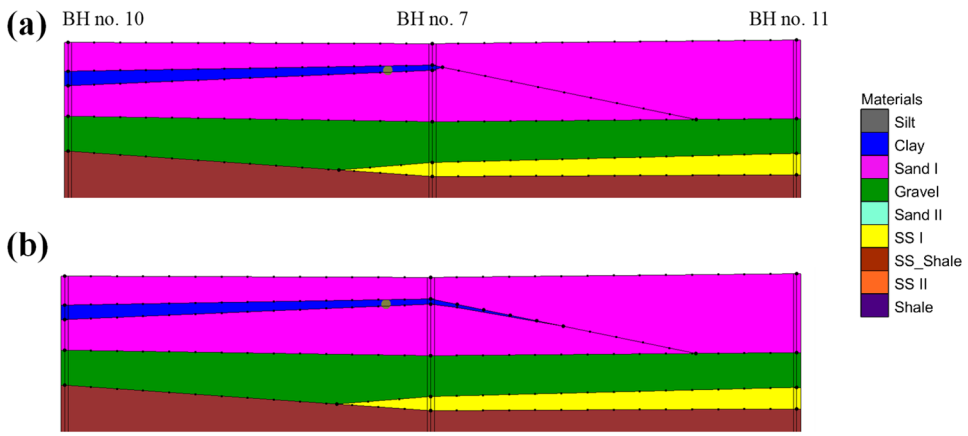

Fig. 6 Comparison of constructed solids (**a**) with and (**b**) without geological knowledge in profile of boreholes nos. 10 to 11. Without geological knowledge, the extension of clay material connects to another formation with an unusual tilt stratum, which may cause uncertainty when the clay material is extrapolated to the whole domain (as done in Fig. 5)

borehole number. As shown, clay thickness based on data from 17 boreholes has a similar pattern to that of SGM. However, in a real engineering geology project, this number of boreholes may be impractical for a 300 m × 300 m site. The geological model uncertainty for a real site is thus high.

Effect of incorporation of geological knowledge

To demonstrate the effect of the incorporation of geological knowledge on a geological model, geological models constructed using data from 17 boreholes with and without

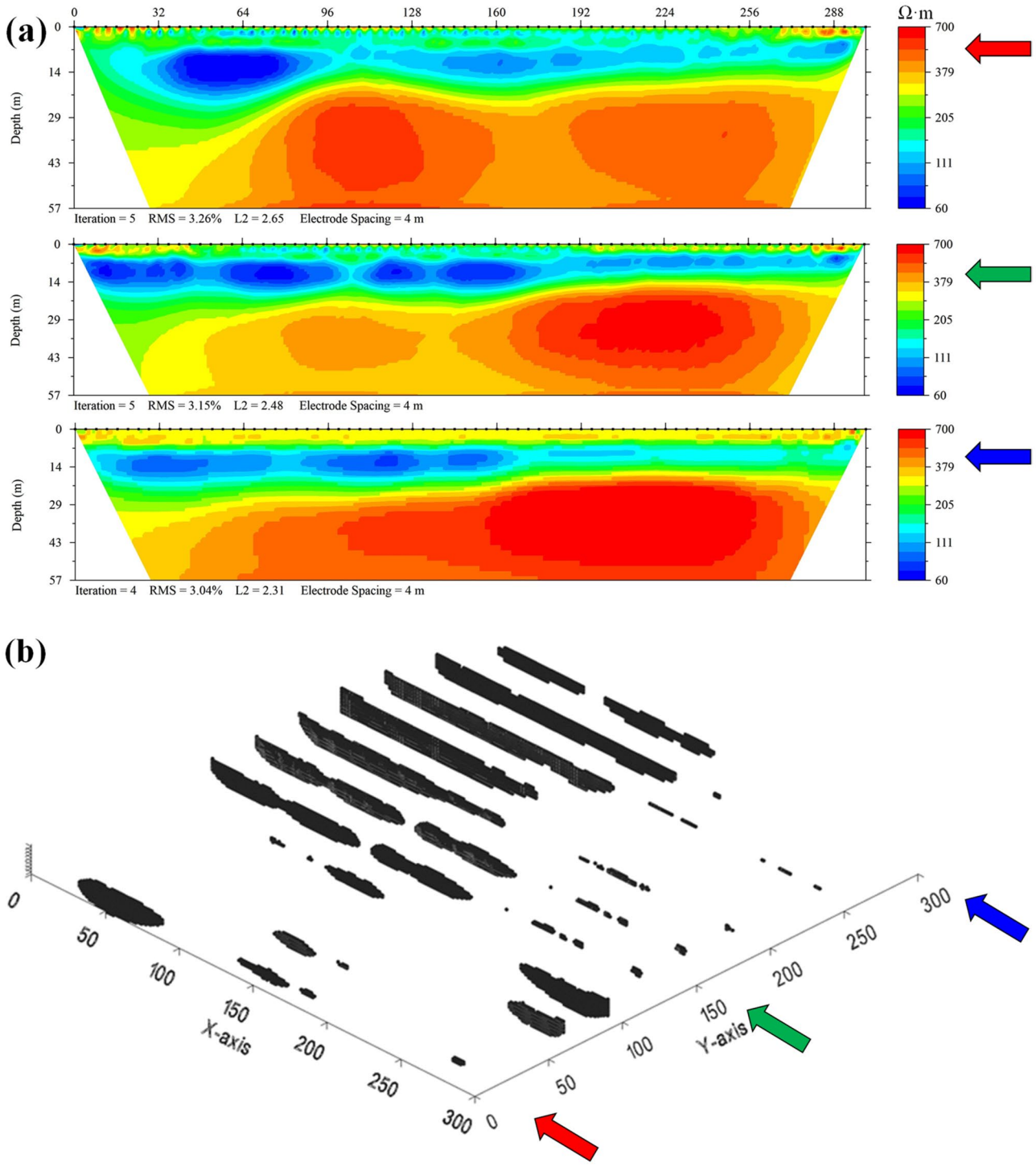

Fig. 7 **a** Example profiles of inverted electrical resistivity model at Y = 0, 150, and 300 m. **b** Estimated clay thickness from ERT data of SGM. Location of the profiles in (**a**) is marked in (**b**) with corresponding color arrow

correction based on geological knowledge were built and compared. The geological cross sections were created by automatically connecting a given material between the boreholes using the horizon ID method, i.e., without the incorporation of geological knowledge. The cross sections were then interpolated into the layer system. Figure 5 shows the distribution of clay thickness for the simulated geological model. This distribution is very different from that of SGM (Fig. 2). Only a small part of the clay thickness has a similar pattern, which is quantitatively different. Compared to the clay thickness estimated using data from 17 boreholes with and without the incorporation of geological knowledge (Figs. 4e and 5, respectively), the simulated geological model with the incorporation of geological knowledge had much better performance.

A profile from borehole nos. 10 to 11 (across no. 7) is shown in Fig. 6 to demonstrate the difference in performance. Note that there are two sets of results, namely a fence diagram (the construction of solids) (Figs. 4e (right) and 6) and a geological interpolation (Figs. 4e (left) and 5). The construction of solids only shows a slight difference in the extension of clay material (Fig. 6), whereas the interpolation results show a large difference due to the uncertainty of clay extrapolation (Figs. 4e (left) and 5). The results demonstrate that including geological knowledge improves the performance of geological models.

Effect of geophysical data assimilation

ERT was performed to identify the clay layers. The obtained clay layers from 11 profiles of the inverted electrical resistivity models were used as an input parameter in the geological model simulation to calculate land subsidence. Two cases, namely one with only ERT data and one with ERT data with correction based on data from 9, 13, and 17 boreholes, are discussed. Data from fewer than 9 boreholes did not yield

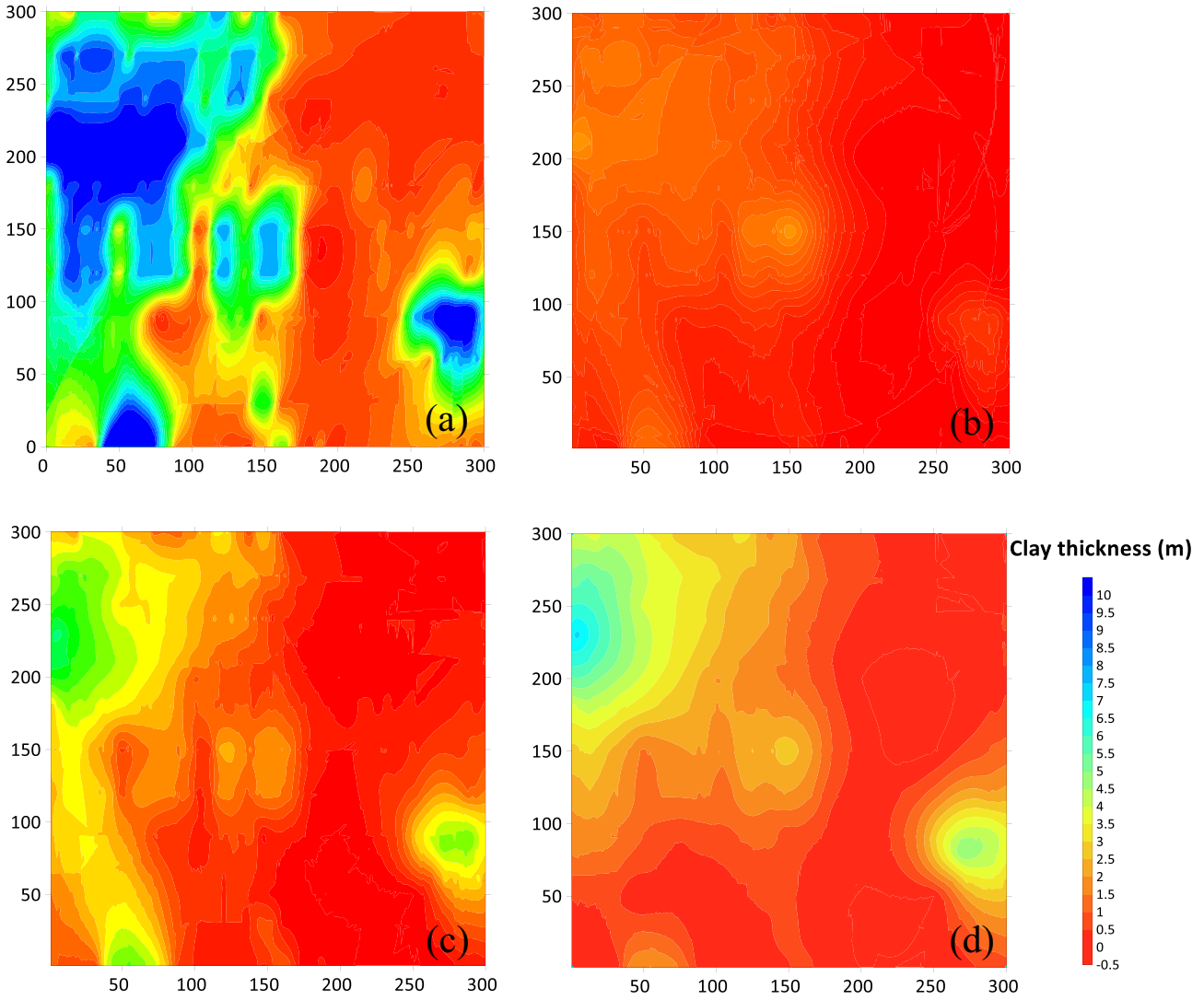

Fig. 8 Distribution of clay thickness for interpolations conducted using **a** ERT data only and ERT data with correction based on data from **b** 9, **c** 13, and **d** 17 boreholes

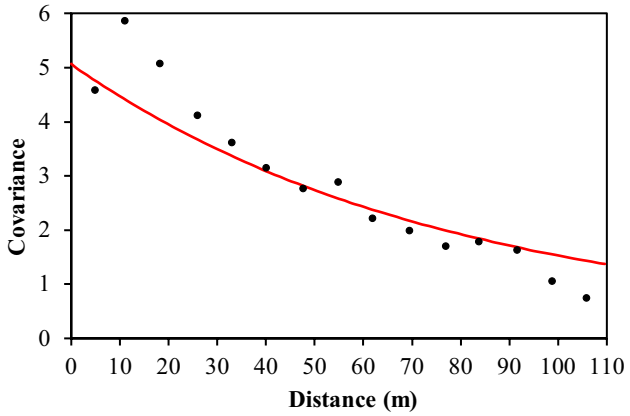

Fig. 9 Cokriging results for ERT data and data from 17 boreholes

reasonable cokriging results. Because the clay thickness estimated from ERT has considerable uncertainty (Doyoro et al. 2021), results obtained with and without the correction were compared to demonstrate the improvement in the geological and numerical models. To assess the effect of adding ERT data in the construction of a geological model, the clay thickness obtained from the simulated geological models was input into SUB to calculate land subsidence.

Use of only ERT data Figure 7 shows the information obtained from ERT models. The electrical resistivity of clay commonly ranges from 0 to 100 Ω m; therefore, this study assumed that in the first aquifer, a grid with electrical resistivity values that range from 0 to 100 Ω m represents clay. Low-electrical-resistivity zones at a shallow depth in the electrical resistivity image thus indicate clay layers. Three example profiles are shown in Fig. 7a. The extracted clay layer information is shown in Fig. 7b. The interpolated ERT clay thickness, shown in Fig. 8a, is larger than that of SGM (Fig. 2). The obtained land subsidence is thus overestimated, leading to unreliable results. Therefore, we used the available borehole information as prior knowledge to constrain the ERT model results.

Use of ERT data with correction based on borehole data To correct the overestimation obtained with the use of ERT data, the cokriging method was used to assimilate geophysical data with data from the geological boreholes. Two clay thickness datasets, namely clay thickness from borehole data and that from ERT data, were used. The two datasets have the same properties, so cokriging is suitable for processing and fitting them. Because the borehole data are sparse and the ERT data are abundant, the former are considered as the target variable and the latter are considered as the supplementary variable in the interpolation. The cokriging results for ERT data and data from 17 geological boreholes are shown in Fig. 9 as an example. The estimated clay thickness obtained from ERT data has a high correlation with that obtained from borehole data. This method reduces the error of estimation based on ERT data.

As mentioned in the previous section, this approach can only be used for models that use data from 9, 13, and 17 boreholes; data from fewer boreholes are insufficient for reasonable results. The calculation results obtained with the corrected clay thickness are shown in Fig. 8b–d. The distribution of clay thickness shows a significant improvement compared

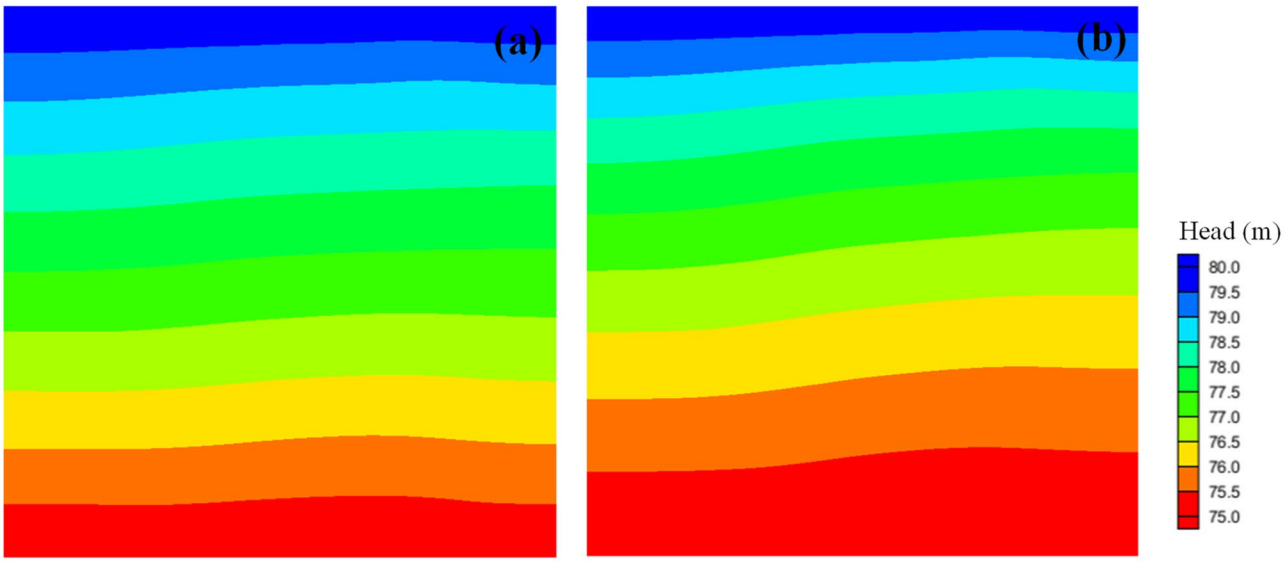

Fig. 10 Groundwater flow results of SGM at **a** 90 days (first period) and **b** 4500 days (last period) in sand I layer

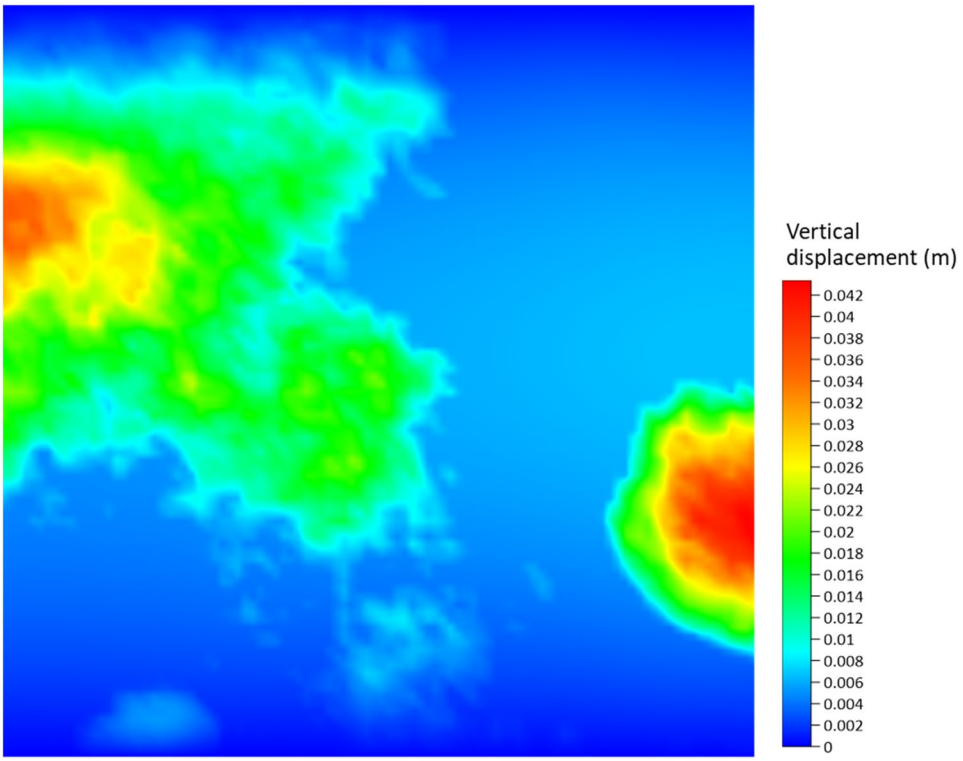

Fig. 11 Vertical displacement results of SGM at 4500 days

to that for the model without correction (Fig. 8a), except for the distribution obtained with the model that used 9 boreholes. The clay thickness for the simulated geological model constructed using only ERT data is much larger than that of SGM at almost every location. The model constructed using cokriging interpolation does not exhibit this overestimation. Specifically, the clay thickness for ERT data with correction based on sufficient borehole data is similar to that of SGM. The numerical results confirm that the use of ERT data with correction based on borehole data yields much better results and thus decreases geological model uncertainty.

Numerical simulation of groundwater flow and land subsidence

Results for SGM

The numerical results of groundwater level in SGM at 90 days and 4500 days are shown in Fig. 10. Groundwater moves from upstream to downstream with relatively stable equipotential lines in the study area. The groundwater level varies from 86 to 73 m based on the boundary condition setting. The groundwater level gradually decreases during the simulation period because of uniform pumping, which causes compaction and thus induces land subsidence.

The numerical results clearly show the effect of clay in the land subsidence calculation, as shown in Fig. 11. The maximum land subsidence is 0.044 m after 4500 days of pumping. At locations with larger clay thickness, land subsidence is more extensive. The results also show the effect of specified head boundary conditions in the numerical model. The land subsidence at the two specified head boundaries is 0 due to a lack of change in groundwater level. This dramatically affects the numerical results of land subsidence as well as the uncertainty of the geological model. Thus, specified head boundary conditions of the groundwater head should be carefully used in land subsidence simulations (Wang and Hsu 2009). Tran et al. (2022) reported that setting the boundary far from the region of interest mitigates the influence of specified head boundary conditions.

Results for models based on data from various numbers of boreholes

The numerical results of groundwater level for simulated geological models based on data from various numbers of boreholes are shown in Fig. 12. All results show a pattern similar to that of SGM (Fig. 10) because the boundary conditions for all simulations were the same and the aquifer system did not significantly change. The changes in groundwater level are similar, which further decreases the influence of groundwater on the calculation of land subsidence.

The results of land subsidence for models based on data from various numbers of boreholes are shown in Fig. 13. The subsidence pattern of these models becomes increasingly

similar to that of SGM with increasing number of boreholes. The simulated geological models based on data from various numbers of boreholes do not significantly influence the groundwater flow model. However, the simulated geological models strongly affect the land subsidence assessment. These comparisons indicate that land subsidence results are strongly affected by the thickness of clay, which is considered to be the interbed in the aquifer. Land subsidence is calculated from the skeletal specific storage, layer thickness, and change in hydraulic head (Eq. (4)). The hydraulic head change is similar for the considered cases and clay has high skeletal specific storage; thus, land subsidence mainly depends on clay thickness. Note that all results are greatly influenced by the specified head boundary conditions of the groundwater

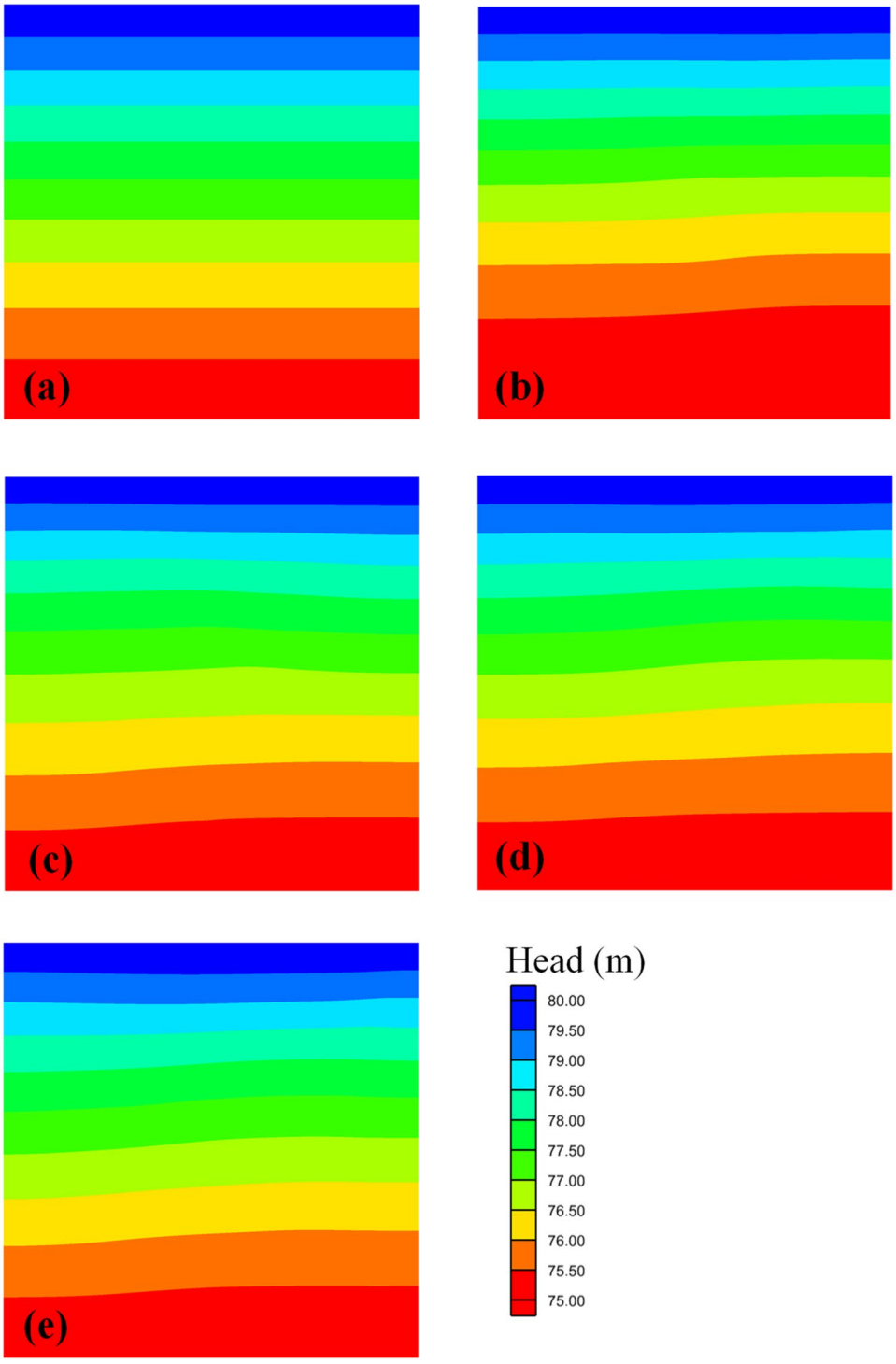

Fig. 12 Groundwater flow results at 4500 days based on simulated geological models based on data from **a** 1, **b** 5, **c** 9, **d** 13, and **e** 17 boreholes obtained with horizon ID method and incorporation of geological knowledge

head, which decrease the land subsidence values and make the results unreasonable near the boundaries.

Results for models with and without geological knowledge incorporation

Because the numerical results of groundwater level are similar between SGM and the simulated geological models, they are not discussed in this or the following section. Figure 14 shows the numerical results of land subsidence obtained using the simulated geological model based on data from 17 boreholes without the incorporation of geological knowledge (Fig. 5). The geological model has poor performance in terms of clay thickness, and thus the results of land subsidence are significantly different from those of SGM. This confirms that geological knowledge should be incorporated into geological models.

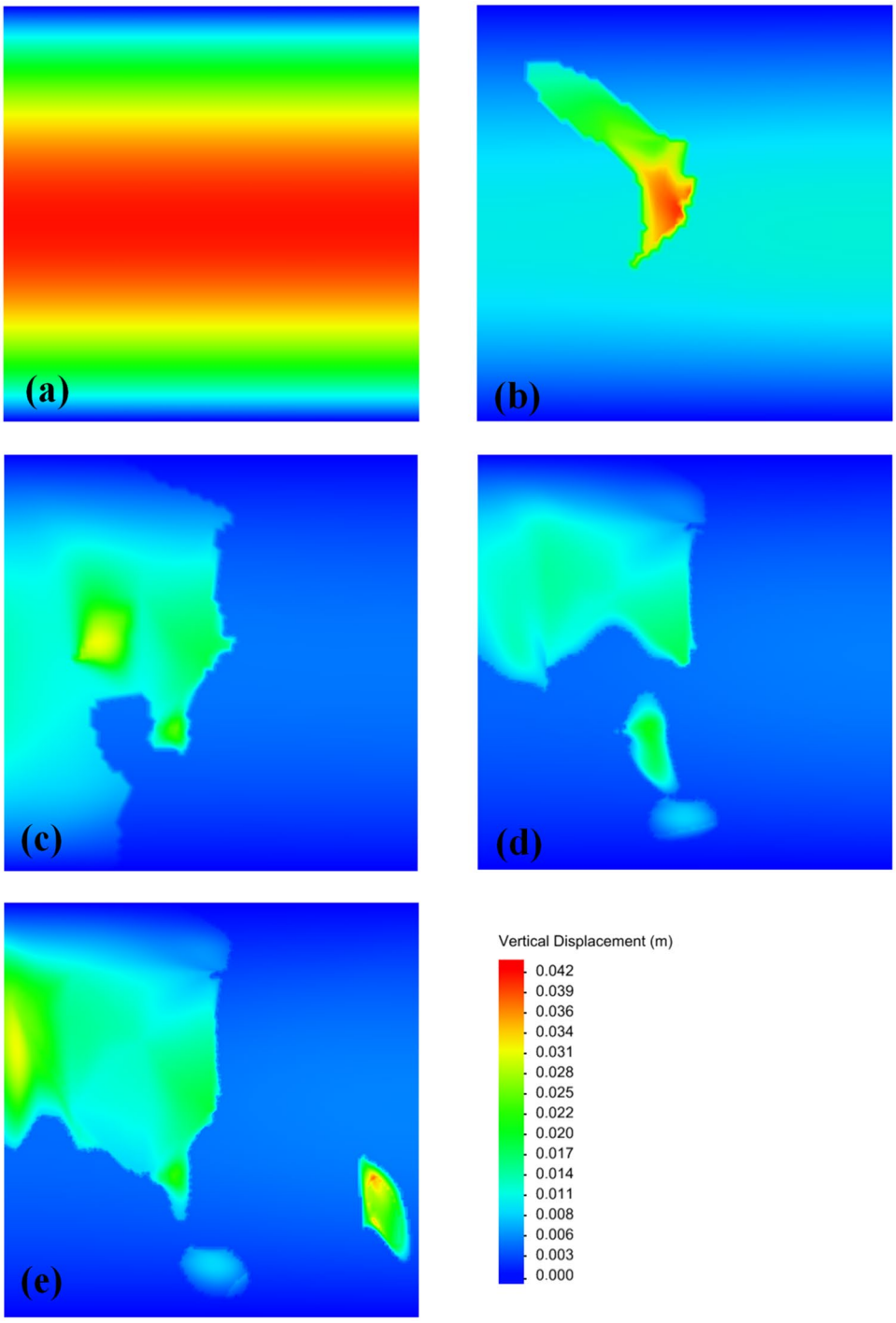

Fig. 13 Land subsidence results at 4500 days based on simulated geological models based on data from **a** 1, **b** 5, **c** 9, **d** 13, and **e** 17 boreholes obtained with horizon ID method and incorporation of geological knowledge

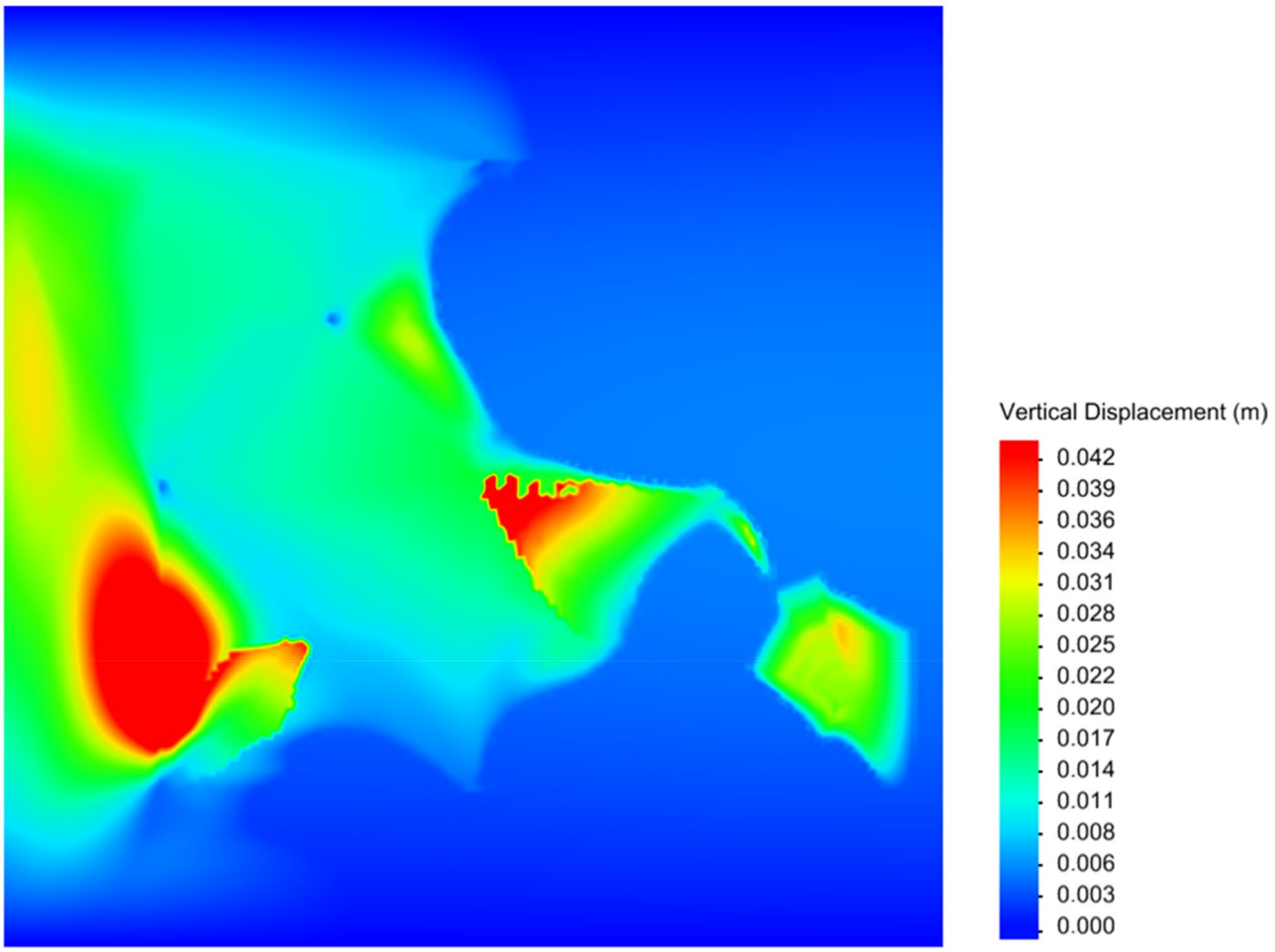

Fig. 14 Land subsidence results at 4500 days based on simulated geological models based on data from 17 boreholes without incorporation of geological knowledge

Results for models with and without geophysical data assimilation

Use of only ERT data Clay thickness in the simulated geological model that uses only ERT data is much higher than that of SGM and thus land subsidence is overestimated (Fig. 15a). The subsidence quantity in the red area is much higher than that of SGM. The results show that adopting the estimated clay thickness from ERT data for land subsidence calculations gives poor results because the results of geophysical surveys commonly embed a significant amount of uncertainty. The calculation results should thus be carefully used.

Use of ERT data with correction based on borehole data The land subsidence results for the simulated geological model that uses ERT data with correction based on data from 13 and 17 boreholes are shown in Fig. 15b, c. The subsidence quantities are lower than those obtained without correction and are thus closer to those of SGM (Fig. 11). The interpolation method was used in the simulated geological model; thus, the distributions of clay thickness and land subsidence are slightly different from those of SGM even though the model gives improved land subsidence results.

Quantification of geological model uncertainty

To quantify the results, the root-mean-square error (RMSE) and coefficient of determination (R^2) are used to assess the difference between the geological models and SGM. The random.sample() function in Python was used to generate 150 random points with a nearly uniform distribution in the study area. The numerical results at these points were used to calculate the RMSE and R^2 values.

A comparison of clay thickness accuracy between the simulated geological models based on data from various numbers of boreholes and SGM is shown in Fig. 16. There is no correlation ($R^2 = 0$) between the model based on data

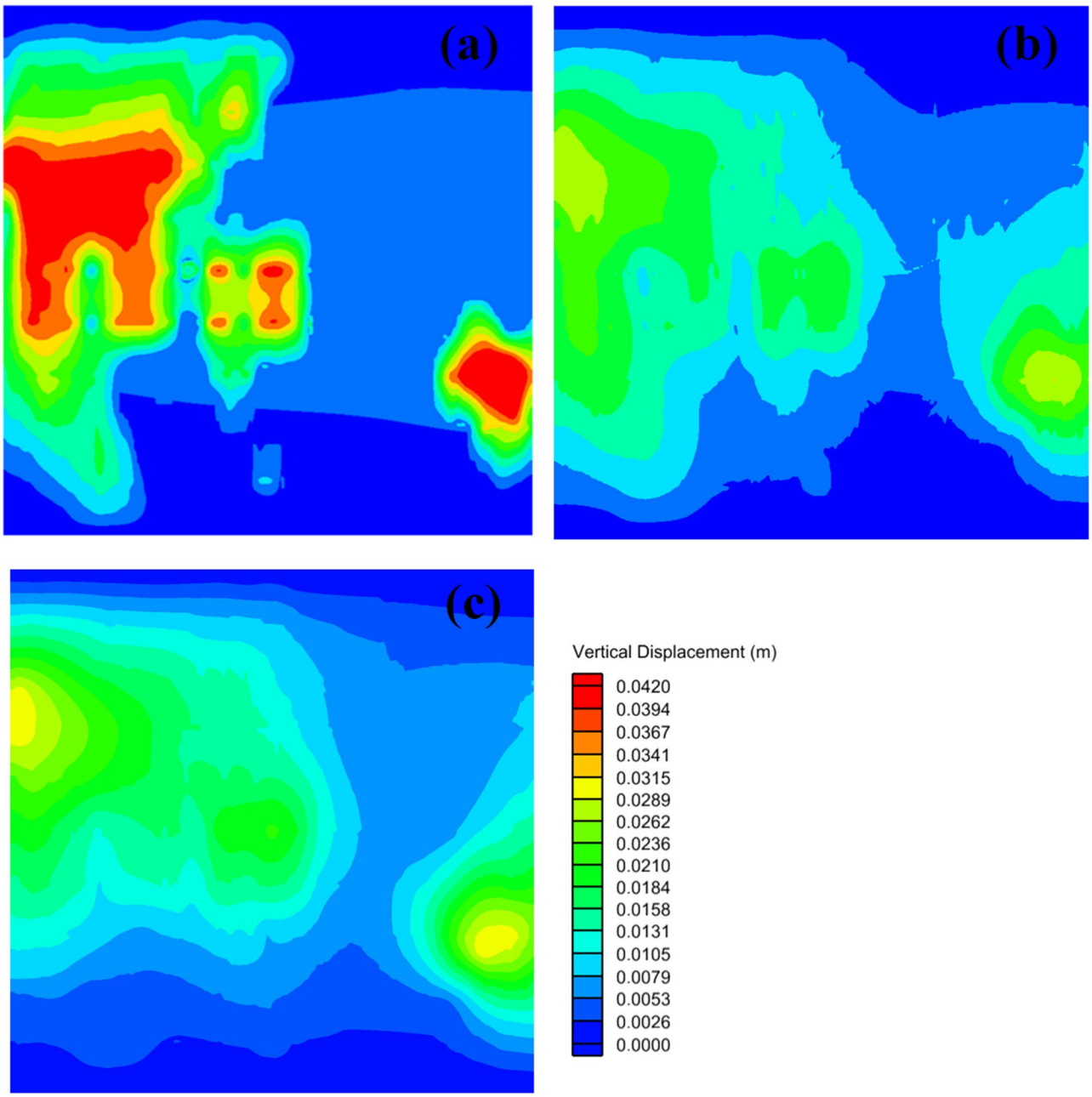

Fig. 15 Land subsidence results at 4500 days based on simulated geological models based on **a** only ERT data and ERT data with correction based on data from **b** 13 and **c** 17 boreholes

from one borehole and SGM. The R^2 values increase with increasing number of boreholes ($R^2 = 0.733$ for 17 boreholes). RMSE decreases from 2.252 m for one borehole to 0.770 m for 17 boreholes. The quantification results show that increasing the number of boreholes in the study area for the geological model construction can decrease uncertainty. The trend is nonlinear and affected by the location of selected boreholes and the distribution of clay.

Figure 17a shows a comparison of the numerical results of groundwater level between the simulated geological models based on data from various numbers of boreholes and SGM. The differences between these results are very small. In all cases, the R^2 value is larger than 0.987 and RMSE is smaller than 0.336 m. This implies that the thickness of the inelastic interbeds in the aquifer system does not significantly affect the numerical results of groundwater level. With an

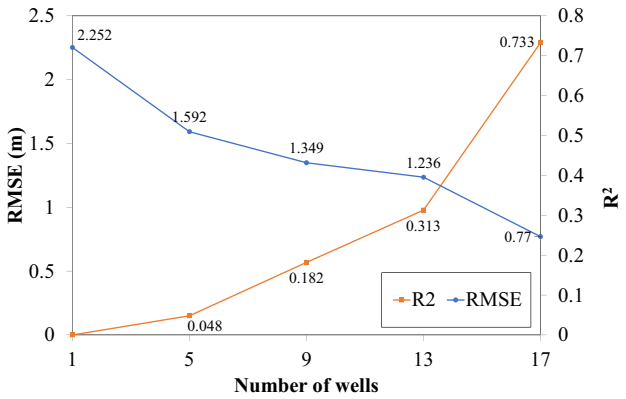

Fig. 16 Comparison of clay thickness accuracy between SGM and simulated geological models based on data from various numbers of boreholes. Blue and orange lines indicate RMSE and R^2, respectively. RMSE decreases from 2.252 to 0.770 m and R^2 value increases from 0 to 0.733 when the borehole number increases from 1 to 17

increase in the number of boreholes, the R^2 value increases and RMSE decreases; their trends are nonlinear. The subsidence results show a similar pattern (Fig. 17b). The numerical results for the model based on data from 17 boreholes have an acceptable RMSE of 4 mm and an R^2 value of 0.787 in the land subsidence simulations (Deng et al. 2017; Mahmoudpour et al. 2016; Zhang et al. 2010). These results can be a reference for engineers and researchers to determine the required borehole number for engineering geology projects at a similar site scale based on the precision requirement.

Figure 18 shows a comparison of the numerical results of land subsidence between the simulated geological model based on data from various levels of data sufficiency and SGM. For the model based on data from 17 boreholes without the incorporation of geological knowledge, the R^2 value slightly increases to 0.316 and RMSE decreases to 7 mm. The results show that the accuracy of this method is very low. The use of data from 17 boreholes and the incorporation of geological knowledge improve the results. The results demonstrate that geological knowledge is necessary for simulating a geological model and land subsidence based on borehole data; its incorporation dramatically increases the accuracy of numerical results and reduces model uncertainty.

The results obtained from the model that used only ERT data show an improvement compared to those for data from boreholes without the incorporation of geological knowledge. The R^2 value is 0.640 and RMSE is 7 mm (Fig. 18).

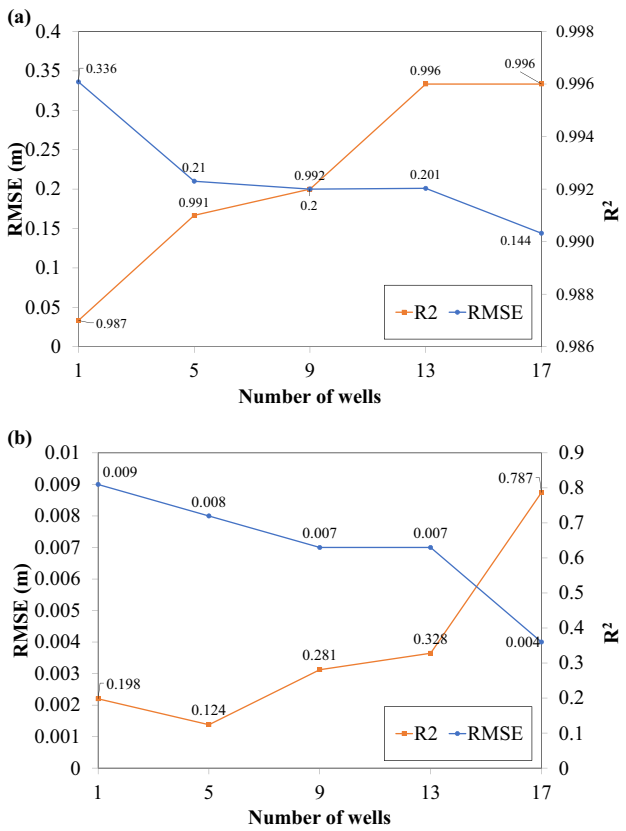

Fig. 17 Comparison of numerical results for **a** groundwater level and **b** land subsidence between SGM and simulated geological models based on data from various numbers of boreholes. Blue and orange lines indicate RMSE and R^2, respectively

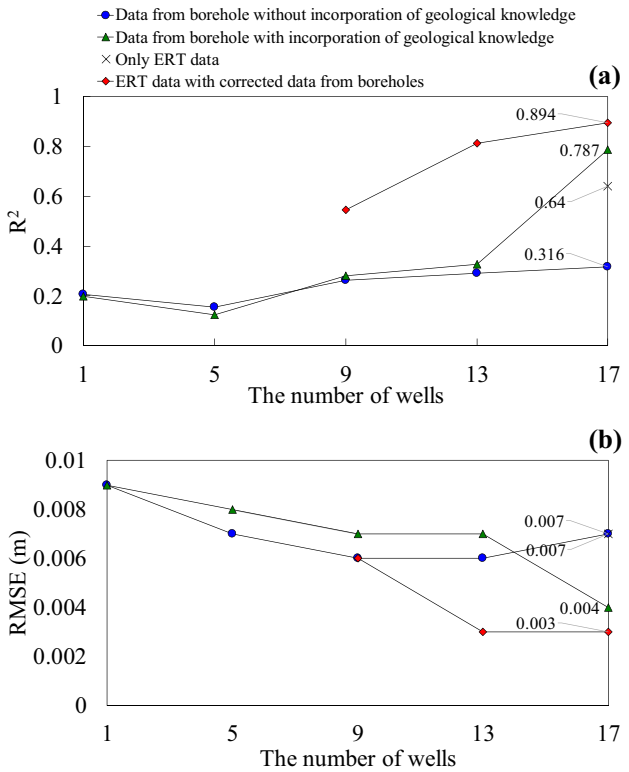

Fig. 18 **a** R^2 and **b** RMSE values of comparison in land subsidence assessment between numerical results obtained from SGM and simulated geological models based on data from boreholes without incorporation of geological knowledge, data from boreholes with incorporation of geological knowledge, only ERT data, and ERT data with corrected data from boreholes

These values are worse than those for the model based on data from 17 boreholes with the incorporation of geological knowledge. Using only ERT data for land subsidence simulation embeds high uncertainty. The results of the simulated geological model that used ERT data with corrected data from 13 and 17 boreholes show a remarkable improvement in the land subsidence simulation. Specifically, the R^2 values are 0.812 and 0.894 and the RMSE values are 3 and 3 mm, respectively (Fig. 18). The results also show higher accuracy than that obtained using 17 boreholes with the incorporation of geological knowledge. The R^2 value increases from 0.787 to 0.894 and RMSE decreases from 4 to 3 mm. The results demonstrate that using data from a limited number of boreholes or only ERT data cannot provide reliable numerical results of land subsidence. A combination of borehole data and ERT data effectively reduces the required well number and uncertainty of geological models and increases numerical model accuracy.

Conclusions

This study performed numerical simulations of groundwater flow and land subsidence for SGM as the baseline. Geological models with various levels of data sufficiency were built. The results from these models were compared with those of SGM to assess the geological model uncertainty. The quantification results show that the clay thickness, groundwater level, and land subsidence results for the model based on borehole data approach those of SGM with increasing borehole number. The model based on data from 17 boreholes that incorporates geological knowledge provided acceptable groundwater flow and land subsidence results for a 300 m × 300 m site. Applying the horizon ID method without the incorporation of geological knowledge yielded assessment results that were far from those of SGM. To increase accuracy and decrease the uncertainty of the geological model, borehole data can be combined with ERT data via the cokriging interpolation method. This combination decreases the required borehole number and yields a dramatic improvement compared with the results obtained using only ERT data or borehole data. The study results can be used by engineers or researchers to determine a suitable strategy for engineering geology projects based on the precision requirements and budget.

From a practical point of view, using 17 boreholes in a 300 m × 300 m site might not be realistic due to cost. Therefore, the influence of geological model uncertainty on numerical simulations will be large. A combination of fewer boreholes (e.g., 13 boreholes) and ERT data can be acceptable for a 300 m × 300 m site, but not in a faulted area, if the relationship between borehole logs and ERT data can be derived. The specified head boundary for groundwater modeling strongly affects the assessment of land subsidence and should be carefully used. Setting the boundary far from the region of interest may mitigate the influence of specified head boundary conditions. In this study, the numerical models were built under the assumption of a layered homogeneous material, making the calculation and simulation process faster and easier. However, materials are commonly not uniformly distributed in a layer but quite heterogeneous. A heterogeneous geological model could be considered in future investigations.

Acknowledgements The authors would like to thank Prof. Chang-Hsein Juang and Prof. Jia-Jyun Dong for providing valuable comments and suggestions to improve the quality of this study. This study was mainly funded by the Shackleton Program "Geological Uncertainty and Societal Risk: the Perspectives of Engineering, Environment, and Geohazards" of the Ministry of Science and Technology, Taiwan (MOST), under grant MOST 108-2638-E-008-001-MY2 and partly funded by MOST under grants MOST 106-2116-M-008-023-MY3 and MOST 110-2123-M-008-001 and the Water Resources Agency, Taiwan, under grants MOEAWRA 1100304 and MOEAWRA 1110346.

Author contribution Shih-Jung Wang: conceptualization, writing—review and editing, validation, discussion, supervision; Quoc Cuong Nguyen: data curation, methodology, software, writing—original draft, discussion; Yu-Chen Lu: methodology, original model creation; Yonatan Garkebo Doyoro: methodology; Duc-Huy Tran: discussion.

Declarations

Competing interests The authors declare no competing interests.

References

Archie GE (1942) The electrical resistivity log as an aid in determining some reservoir characteristics. Transactions of the AIME 14601:54–62

Benedek K, Molnár P (2013) Combining structural and hydrogeological data: Conceptualization of a fracture system. Eng Geol 163:1–10

Boyd DL, Walton G, Trainor-Guitton W (2019) Quantifying spatial uncertainty in rock through geostatistical integration of borehole data and a geologist's cross-section. Eng Geol 260:105246

Bredehoeft J (2005) The conceptualization model problem—surprise. Hydrogeol J 131:37–46

Bredehoeft JD (2003) From models to performance assessment: the conceptualization problem. Groundwater 415:571–577

Carrera J, Alcolea A, Medina A, Hidalgo J, Slooten LJ (2005) Inverse problem in hydrogeology. Hydrogeol J 131:206–222

Chiles J-P, Aug C, Guillen A, Lees T (2004) Modelling the geometry of geological units and its uncertainty in 3D from structural data: the potential-field method. Proceedings of international symposium on orebody modelling and strategic mine planning, Perth, Australia, Citeseer

De Loera J, Rambau J, Santos F (2010) Triangulations: structures for algorithms and applications. Berlin, Germany

Deng Z, Ke Y, Gong H, Li X, Li Z (2017) Land subsidence prediction in Beijing based on PS-InSAR technique and improved Grey-Markov model. Giscience Remote Sensing 54(6):797–818. https://doi.org/10.1080/15481603.2017.1331511

Doyoro YG, Chang P-Y, Puntu JM (2021) Uncertainty of the 2D resistivity survey on the subsurface cavities. J Appl Sci 11(7):3143
Fan Y, Huang GH, Baetz BW, Li Y, Huang K, Li Z, Chen X, Xiong L (2016) Parameter uncertainty and temporal dynamics of sensitivity for hydrologic models: A hybrid sequential data assimilation and probabilistic collocation method. Environ Model Softw 86:30–49
Fournier A, Fussell D, Carpenter L (1982) Computer rendering of stochastic models. Commun ACM 256:371–384
Gallagher M, Doherty J (2007) Parameter estimation and uncertainty analysis for a watershed model. Environ Model Softw 227:1000–1020
Gong W, Zhao C, Juang CH, Tang H, Wang H, Hu X (2020) Stratigraphic uncertainty modelling with random field approach. Computers Geotechnics 125:103681. https://doi.org/10.1016/j.compgeo.2020.103681
Guillaume JH, Qureshi ME, Jakeman AJ (2012) A structured analysis of uncertainty surrounding modeled impacts of groundwater-extraction rules. Hydrogeol J 205:915–932
Harbaugh AW, Banta ER, Hill MC, McDonald MG (2000) MODFLOW-2000, the U.S. geological survey modular ground-water model-user guide to modularization concepts and the groundwater flow process. Open-file report. U.S. Geological Survey 92:134.https://doi.org/10.3133/ofr200092
Hassan AE, Bekhit HM, Chapman JB (2008) Uncertainty assessment of a stochastic groundwater flow model using GLUE analysis. J Hydrol 3621–2:89–109
Hoffmann J, Leake SA, Galloway DL, Wilson AM (2003) MODFLOW-2000 ground-water model–User guide to the subsidence and aquifer-system compaction (SUB) package. Open-File Report u s Geological Survey 03:233
Højberg A, Refsgaard J (2005) Model uncertainty–parameter uncertainty versus conceptual models. Water Sci Technol 526:177–186
Hong QX (2011) Using MODFLOW associated with SUB package to predict vertical average of long-term land subsidence in Yunlin. National Central University, Taiwan
Jacob CE (1940) On the flow of water in an elastic artesian aquifer. EOS Trans Am Geophys Union 212:574–586
Johnson AI (1967) Specific yield: compilation of specific yields for various materials. D.C., United States, Washington
Juang CH, Zhang J, Shen M, Hu J (2019) Probabilistic methods for unified treatment of geotechnical and geological uncertainties in a geotechnical analysis. Eng Geol 249:148–161
Kanli AI, Neducz B (2015) Electromagnetic measurements for monitoring molybdenum contamination in near-surface survey. Earth Sci Res J 19(2):107–111
Leake S (1990) Interbed storage changes and compaction in models of regional groundwater flow. Water Resour Res 269:1939–1950. https://doi.org/10.1029/WR026i009p01939
Lelliott M, Cave M, Wealthall G (2009) A structured approach to the measurement of uncertainty in 3D geological models. Q J Eng Geol Hydrogeol 421:95–105. https://doi.org/10.1144/1470-9236/07-081
Lemon AM, Jones NL (2003) Building solid models from boreholes and user-defined cross-sections. Comput Geosci 295:547–555
Li Z, Wang X, Wang H, Liang RY (2016) Quantifying stratigraphic uncertainties by stochastic simulation techniques based on Markov random field. Eng Geol 201:106–122
Liu X, Wang Y, Yan S, Shao Y, Zhou H, Li Y (2019) Ground subsidence characteristics associated with urbanization in East China analyzed with a Sentinel-1A-based InSAR time series approach. Bull Eng Geol Env 786:4003–4015. https://doi.org/10.1007/s10064-018-1383-6
Loke MH, Acworth I, Dahlin T (2003) A comparison of smooth and blocky inversion methods in 2D electrical imaging surveys. Explor Geophys 34(3):182–187
Mahmoudpour M, Khamehchiyan M, Nikudel MR, Ghassemi MR (2016) Numerical simulation and prediction of regional land subsidence caused by groundwater exploitation in the southwest plain of Tehran. Iran Engineering Geology 201:6–28. https://doi.org/10.1016/j.enggeo.2015.12.004
Marinoni O (2003) Improving geological models using a combined ordinary–indicator kriging approach. Eng Geol 691–2:37–45
McDonald MG, Harbaugh AW (1988) A modular three-dimensional finite-difference ground-water flow model: U.S. Geological Survey Techniques of Water Resources Investigations
Meinzer OE (1928) Compressibility and elasticity of artesian aquifers. Econ Geol 233:263–291
Moradkhani H, Hsu KL, Gupta H, Sorooshian S (2005) Uncertainty assessment of hydrologic model states and parameters: Sequential data assimilation using the particle filter. Water Resour Res 415
Neuman SP (2003) Maximum likelihood Bayesian averaging of uncertain model predictions. Stoch Env Res Risk Assess 175:291–305
Nyári Z, Kanlı AI (2007) Imaging of buried 3D objects by using electrical profiling methods with GPR and 3D geoelectrical measurements. J Geophys Eng 4(1):83–93
Nyári Z, Kanlı AI, Stickel J, Tillmann A (2010) The use of non-conventional CPTe data in determination of 3-D electrical resistivity distribution. J Appl Geophys 70(3):255–265
Qi X-H, Li D-Q, Phoon K-K, Cao Z-J, Tang X-S (2016) Simulation of geologic uncertainty using coupled Markov chain. Eng Geol 207:129–140
Qi X-H, Liu H-X (2019) An improved global zonation method for geotechnical parameters. Eng Geol 248:185–196
Refsgaard JC, Christensen S, Sonnenborg TO, Seifert D, Højberg AL, Troldborg L (2012) Review of strategies for handling geological uncertainty in groundwater flow and transport modeling. Adv Water Resour 36:36–50
Refsgaard JC, Van der Sluijs JP, Brown J, Van der Keur P (2006) A framework for dealing with uncertainty due to model structure error. Adv Water Resour 2911:1586–1597
Rojas R, Feyen L, Dassargues A (2008) Conceptual model uncertainty in groundwater modeling: Combining generalized likelihood uncertainty estimation and Bayesian model averaging. Water Resour Res 4412
Rubin Y, Hubbard SS (2006) Hydrogeophysics. Berlin, Germany
Rushton KR, Redshaw SC (1979) Seepage and groundwater flow: Numerical analysis by analog and digital methods
Shi X, Fang R, Wu J, Xu H, Sun Y, Yu J (2012) Sustainable development and utilization of groundwater resources considering land subsidence in Suzhou, China. Eng Geol 124:77–89
Shi X, Wu J, Ye S, Zhang Y, Xue Y, Wei Z, Li Q, Yu J (2008) Regional land subsidence simulation in Su-xi-Chang area and Shanghai City, China. Eng Geol 1001–2:27–42
Tao Y, Sun H, Cai Y (2020) Predicting soil settlement with quantified uncertainties by using ensemble Kalman filtering. Eng Geol 276:105753
Terzaghi K (1925) Principles of Soil Mechanics Engineering News-Record 9519–27:19–32
Tildy P, Neducza B, Nagy P, Kanli AI, Hegymegi C (2017) Time lapse 3D geoelectric measurements for monitoring of in-situ remediation. J Appl Geophys 136:99–113
Tran D-H, Wang S-J, Nguyen QC (2022) Uncertainty of heterogeneous hydrogeological models in groundwater flow and land subsidence simulations—a case study in Huwei Town. Taiwan Engineering Geology 298:106543
Tsai VJ (1993) Delaunay triangulations in TIN creation: an overview and a linear-time algorithm. Int J Geogr Inf Sci 76:501–524
Vrugt JA, Diks CG, Gupta HV, Bouten W, Verstraten JM (2005) Improved treatment of uncertainty in hydrologic modeling: Combining the strengths of global optimization and data assimilation. Water Resour Res 411

Wang H, Wellmann JF, Li Z, Wang X, Liang RY (2017a) A segmentation approach for stochastic geological modeling using hidden Markov random fields. Math Geosci 492:145–177

Wang S-J, Lee C-H, Hsu K-C (2015) A technique for quantifying groundwater pumping and land subsidence using a nonlinear stochastic poroelastic model. Environmental Earth Sciences 7312:8111–8124. https://doi.org/10.1007/s12665-014-3970-6

Wang S-J, Lee C-H, Yeh C-F, Choo YF, Tseng H-W (2021) Evaluation of climate change impact on groundwater recharge in groundwater regions in Taiwan. Water 13(9):1153

Wang S-J, Hsu K-C (2009) The application of the first-order second-moment method to Analyze poroelastic problems in heterogeneous porous media. J Hydrol 369(1–2):209–221

Wang X, Wang H, Liang RY (2018) A method for slope stability analysis considering subsurface stratigraphic uncertainty. Landslides 155:925–936

Wang Y, Akeju OV, Zhao T (2017b) Interpolation of spatially varying but sparsely measured geo-data: a comparative study. Eng Geol 231:200–217

Yao Y, Zhang M, Deng Y, Dong Y, Wu X, Kuang X (2021) Evaluation of environmental engineering geology issues caused by rising groundwater levels in Xi'an, China. Eng Geol 106350

Yeh C-H, Dong J-J, Khonevisan S, Juang CH, Huang W-C, Lu Y-C (2021) The role of the geological uncertainty in a geotechnical design–A retrospective view of Freeway No. 3 Landslide in Northern Taiwan. Eng Geol 106233

Zhang Q-L, Chen Y-X, Jilani G, Shamsi IH, Yu Q-G (2010) Model AVSWAT apropos of simulating non-point source pollution in Taihu lake basin. J Hazard Mater 174(1–3):824–830

Zhao T, Xu L, Wang Y (2020) Fast non-parametric simulation of 2D multi-layer cone penetration test (CPT) data without pre-stratification using Markov Chain Monte Carlo simulation. Eng Geol 273:105670